Design and Experiment Results of High-Speed Wireless Link Using Sub-terahertz Wave Generated by Photonics-Based Technology

Sungil Kim, Seung-Ho Ahn, and Seong Su Park

Using a sub-terahertz (sub-THz) wave generated using a photonics-based technology, a high-speed wireless link operating at up to 10 Gbps is designed and demonstrated for realization of seamless connectivity between wireless and wired networks. The sub-THz region is focused upon because of the possibility to obtain sufficient bandwidth without interference with the allocated RF bands. To verify the high-speed wireless link, such dynamic characteristics as the eye diagrams and bit error rate (BER) are measured at up to 10 Gbps for non-return-to-zero pseudorandom binary sequence 2^{31}–1 data. From the measurement results, a receiver sensitivity of –23.5 dBm at BER=10^{-12} is observed without any error corrections when the link distance between the transmitter and receiver is 3 m. Consequently, we hope that our design and experiment results will be helpful in implementing a high-speed wireless link using a sub-THz wave.

Keywords: High-speed, wireless link, sub-terahertz, photonic-based technology.

I. Introduction

The terahertz (THz) frequency range, which is from 100 GHz to 10 THz, lies in the frequency gap between infrared and microwave wavelengths [1]. The properties and propagation characteristics of THz waves are shorter wavelengths for imaging applications with sufficient spatial resolution, unlicensed spectrum with wide bandwidths in the case of radio communication, transparency for non-metal materials, and the existence of a substance-intrinsic (gas, liquid, and solid) spectrum.

This range has rarely been used for commercial applications owing to a lack of cost-effective sources and detectors [2]. Today, based on innovations and breakthroughs in photonics and nanotechnology, THz sources and detectors are feasible with reasonable cost and reliable performances for commercial products. THz time-domain spectroscopy and THz imaging systems were introduced to analyze the scientific behaviors of materials and to secure human safety [3], [4].

One of the candidate application fields is a high-speed wireless link because of its possibility to obtain a sufficient bandwidth without interference with the allocated RF bands. A high-speed wireless link can be applicable to a wireless backhaul and seamless connectivity between wired and wireless networks as fixed wireless access. Such a link can apply to the transfer of high-quantity data, such as high-definition multimedia files from a personal information terminal to a storage device. To implement a high-speed wireless link, the sub-THz range, which is from 100 GHz to 1 THz, is focused upon, owing to a lower atmospheric loss gap,

Manuscript received Nov. 30, 2012; revised Mar. 22, 2013; accepted May 6, 2013.

Sungil Kim (phone: +82 42 860 6798, silkim@etri.re.kr, sungilkim69@gmail.com) and Seong Su Park (sspark@etri.re.kr) are with the Creative Future Research Laboratory, ETRI, Daejeon, Rep. of Korea.

Seung-Ho Ahn (shahn@etri.re.kr) is with the Components & Materials Research Laboratory, ETRI, Daejeon, Rep. of Korea.

http://dx.doi.org/10.4218/etrij.13.1912.0017

such as at around 100 GHz, 240 GHz, and 400 GHz [5], [6].

A key component to realizing a high-speed wireless link using a sub-THz wave is a stable continuous wave (CW) generator [7]-[9]. In terms of the method used to make a CW generator, a high-speed wireless link can be distinguished between those based on photonics and those based on electronics technology [8]. In the case of a sub-THz CW generator based on electronics, a frequency multiplier scheme is usually researched using InP, GaAs, SiGe, and Si technologies [10]-[16]. In addition, there has been a great deal of research activity in generating a sub-THz CW based on photonics, such as quantum cascade lasers [17]-[21] and photomixing two lightwaves with different wavelengths [7], [8], [17], [22], [23]. This is because there are certain advantages, such as a wider tunability, narrower spectral linewidth, and lower degree of implementation difficulty than electronics-based technology.

In photonics-based technology, photomixing has been widely studied in attempts to make a sub-THz CW because of several advantages, such as a high spectral purity, desirable frequency tunability, narrow spectral linewidth, and room-temperature operation, in comparison with the same qualities of the other schemes [7], [8], [17], [22], [23]. One of the well-known photomixing techniques is a usual double sideband-suppressed carrier (DSB-SC) scheme, which can easily obtain two strongly correlated lightwaves with relatively simple configurations.

Accordingly, a sub-THz transmitter (Tx) based on photonics-based technology is implemented to design and demonstrate a high-speed wireless link. A sub-THz Tx is composed of a photonic oscillator based on the usual DSB-SC scheme, a modulator, and a sub-THz generator. The photonic oscillator generates two correlated lightwaves with wavelength differences, which correspond to the frequency of the desired sub-THz wave. The output of the photonic oscillator is modulated with data on the modulator. The sub-THz generator then gives rise to and radiates the wanted sub-THz wave. A sub-THz receiver (Rx), which is an envelope detector, consists of a Schottky barrier diode (SBD) and pre- and post-amplifiers.

Using optical and electrical spectrum analyzers and an oscilloscope, the sub-THz Tx is verified for the frequency and the time domain. The fiber-optic components operating in wavelength ranges of 1,550 nm are used to generate a 120-GHz CW. With non-return-to-zero (NRZ) pseudorandom binary sequence (PRBS) 2^{31}–1 data, an eye diagram of 10 Gbps is observed to evaluate the modulator. The performances of the sub-THz Rx are also verified using a back-to-back test with the sub-THz Tx. Dynamic performances such as the eye diagrams and bit error rate (BER) are measured with a link distance of 3 m between the sub-THz Tx and the sub-THz Rx. A receiver sensitivity of –23.5 dBm at BER=10^{-12} with 10-Gbps NRZ PRBS 2^{31}–1 data is observed without any error corrections. Accordingly, we find that a high-speed wireless link using the sub-THz wave based on photonics-based technology is feasible.

In [24], there were some filters, such as a planar lightwave circuit, that integrated an arrayed waveguide grating and 3-dB coupler with an optical bandpass filter before a photomixer to increase the spectral purity of a sub-THz CW. A clock-data recovery and an electro-optic conversion circuitry for error corrections were also used to improve the eye diagrams and BER performances. In this work, a single wavelength laser is used, whereas two discrete wavelength-tunable lasers were used to make a sub-THz CW in [25]. Accordingly, a stabilizer should have been applied in [25] to ensure correlations between two discrete wavelength-tunable lasers for stable performances of the wireless link.

Based on our experiment results, we find it feasible that more cost-effective solutions for a high-speed wireless link using a sub-THz wave can be implemented without an error correction scheme, high-cost filters, and a stabilizer compared to that of previous work [24], [25]. Consequently, we hope that our design and experiment results can be helpful to realize a high-speed wireless link using the sub-THz wave.

II. Design Concepts of Sub-THz Tx and Rx

A block diagram of the sub-THz Tx based on photonics-based technology is shown in Fig. 1. The sub-THz Tx consists of a photonic oscillator, a modulator, and a sub-THz generator. The photonic oscillator, which is configured using a usual DSB-SC scheme, emits two strongly correlated lightwaves with wavelength differences corresponding to the wanted sub-THz frequency (f_{THz}). The lightwaves go to the modulator and are modulated with the data. The modulated sub-THz wave is generated at the sub-THz generator after photomixing them and radiated into free space. To use mature fiber-optic technologies, which have been well developed in optical communication fields, such as fiber-to-the-home services, fiber-optic components with wavelengths of 1,550 nm are applied to the sub-THz Tx. A polarization-maintaining fiber (PMF) technique is included to suppress the loss produced from polarization mismatches between lightwaves.

The photonic oscillator is composed of an optical source, an optical intensity modulator (IM), a local oscillator (LO), and an erbium-doped fiber amplifier (EDFA), as illustrated in Fig. 2, with its verification setup. The terms f_{LO}, λ_C, P_C, λ_S, and $P_{DSB\text{-}SC}$ are the frequency of the LO, the wavelength and power of the optical carrier emitted by the optical source, and the wavelength and power of the double sideband (DSB) signals,

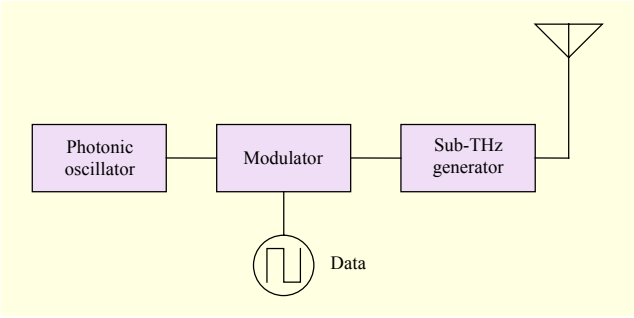

Fig. 1. Block diagram of sub-THz Tx based on photonics-based technology.

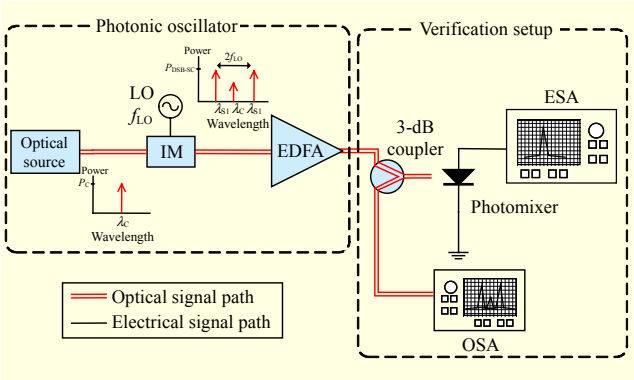

Fig. 2. Schematic of photonic oscillator with verification setup.

respectively. To make the DSB signals, the optical carrier is modulated with the frequency and power of the LO on the IM. Based on the work in [26] and [27], the DSB-SC signals are completed by suppressing the optical carrier using the null-biased IM. The EDFA then amplifies the DSB-SC signals to increase the power of the sub-THz wave generated by photomixing the DSB-SC signals.

The verification setup consists of the following: a 2×1 3-dB coupler; a photomixer, which operates with a reverse bias voltage; an electrical spectrum analyzer (ESA); and an optical spectrum analyzer (OSA). The 2×1 3-dB coupler splits the output of the EDFA into two paths. One goes to the OSA to verify the optical performances of the photonic oscillator. The other goes to the photomixer with the ESA to generate and measure the sub-THz wave.

Using the sum of the square roots and Cartesian coordinates, the instantaneous electric field intensities of the photomixed output power ($\tilde{E}_{\mathrm{ph}}(0,t)$) of the photonic oscillator can be approximately expressed, as in [28] and [29], as

$$\begin{aligned}\tilde{E}_{\mathrm{Ph}}(0,t) &= \left(E_{\mathrm{S},x}{}^2 + E_{\mathrm{S},y}{}^2\right)\cos\left(4\pi f_{\mathrm{LO}}t\right) \\ &+2\left(E_{\mathrm{S},x}E_{\mathrm{C},x} + E_{\mathrm{S},y}E_{\mathrm{C},y}\right)\cos\left(2\pi f_{\mathrm{LO}}t\right) \\ &+The\_Others, \end{aligned} \quad (1)$$

where $E_{S,x}$, $E_{S,y}$, $E_{C,x}$, and $E_{C,y}$ are the x- and y-axis components

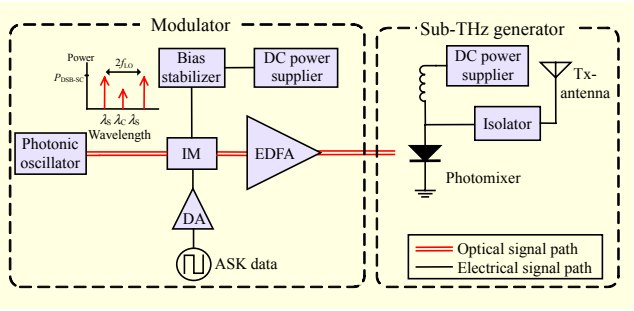

Fig. 3. Schematic of modulator and sub-THz generator of sub-THz Tx.

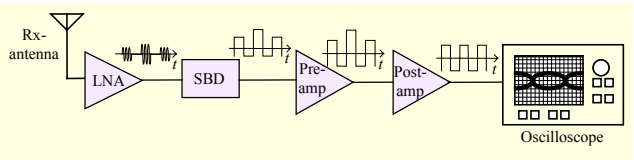

Fig. 4. Block diagram of sub-THz Rx.

of the DSB signals and the optical carrier, respectively. *The_Others* includes the optical rectification (DC terms), the second harmonics, and the sum frequency terms. The second harmonics and the sum frequency terms, which have a frequency of over 100 THz, are out of the sub-THz range Accordingly, *The_Others* can be negligible. The first term is the wanted sub-THz wave, which has a frequency corresponding to a wavelength difference between DSB signals. The second term is noise, which is induced by the optical carrier. From (1), we find that the optical carrier should be sufficiently suppressed to minimize the noise term.

Figure 3 shows a schematic of the modulator and the sub-THz generator of the sub-THz Tx. The modulator modulates the DSB-SC signals with the amplitude shift keying (ASK) data. It is simply composed of the following: a DC power supplier; an IM with a bias stabilizer; a drive amp (DA), which amplifies the ASK data for sufficient operation of the IM up to 10 Gbps; and an EDFA, which is used to compensate for the insertion loss of the IM. The sub-THz generator consists of a photomixer, a DC power supplier, an isolator, and a Tx-antenna. The modulated output of the modulator goes to the photomixer. The sub-THz wave with the ASK modulated data is then generated through photomixing and radiated by the Tx-antenna. The isolator is used to protect the photomixer against reflected waves occurring from an impedance mismatch between the photomixer and Tx-antenna.

Figure 4 shows a block diagram of the sub-THz Rx, which is composed of a Rx-antenna, a low-noise amplifier (LNA), an SBD, a pre-amplifier, and a post-amplifier. The received sub-THz wave by the Rx-antenna is first amplified by the LNA. An envelope of the received sub-THz wave is detected by the SBD.

The envelope of the received sub-THz wave is then amplified by the pre-amplifier and the post-amplifier. Finally, the received sub-THz wave is measured and verified using an oscilloscope and a BER tester in the time domain.

III. Experiment Results

Using the LO with f_{LO}=60 GHz and +20-dBm output power, DSB-SC signals separated by 120 GHz (2 f_{LO}) are generated. The half-wave voltage of the IM using a Mach-Zehnder interferometer (MZI) is 3.5 V. The PMF components with matched optical connectors, such as the IM and passive components operating at 1,550 nm, are used to increase the operation stability and reduce the polarization and connector mismatch losses. To verify the photonic oscillator, a 120-GHz CW as the sub-THz CW is generated by the photomixer, which is a uni-traveling carrier photodiode (UTC-PD) made by NEL Electronics. The UTC-PD with PMF pigtailing and a WR-8 waveguide output is reverse-biased at –2 V and operates in the F-band (90 GHz to 140 GHz).

The photomixed output power (P_{Ph}) of the generated 120-GHz CW by photomixing the output of the photonic oscillator is shown in Fig 5. This result is directly related to the characteristics of the photomixer. The ESA with a harmonic mixer (HM), which is made by OML Inc., is used for measuring the generated 120-GHz CW. In this figure, I_{ph}, $P_{Ph,Cal}$, Read-Out, and $P_{Ph,meas}$ are the photocurrent of the photomixer when the lightwaves are inserted, the calculated photomixed output power to confirm the measured results, the read-out value from the datasheet of the photomixer, and the measured photomixed output power with a 50-dB conversion loss of the HM, respectively. The calculated photomixed output power according to the power of the DSBs is expressed through (2) [30]:

$$P_{\mathrm{Ph,Cal}}\left(\mathrm{dBm}\right)=\left(R_{\mathrm{DC}}\rho\sqrt{2P_{\mathrm{S}}^{2}}\right)\times Z_{0}\,, \tag{2}$$

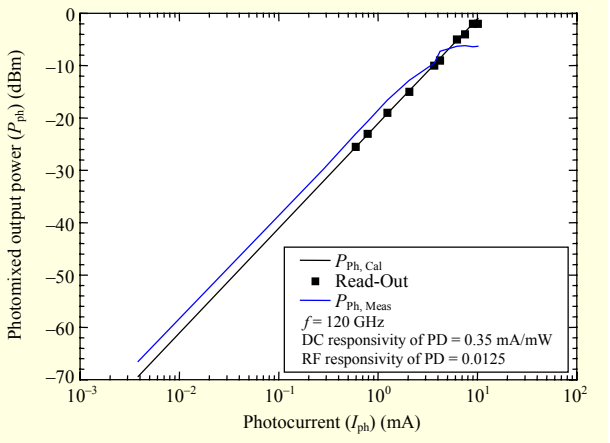

Fig. 5. Photomixed output power of generated 120-GHz CW through photomixing.

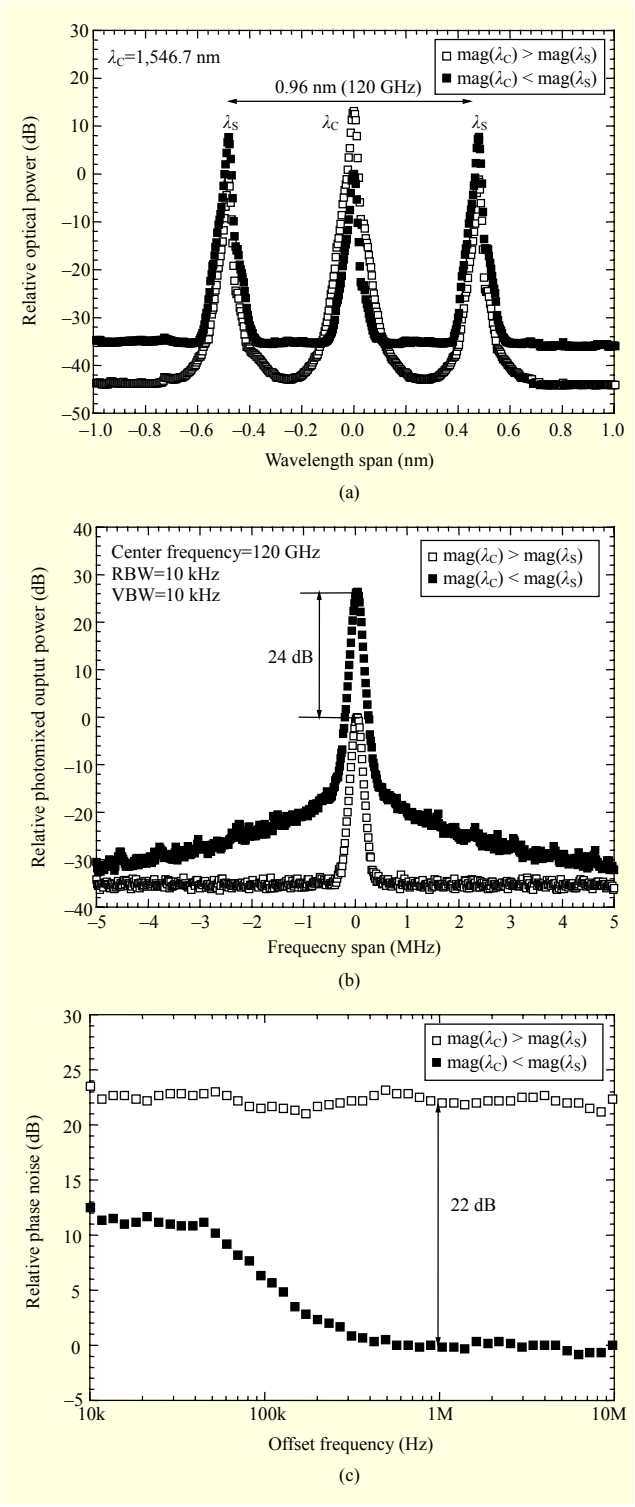

Fig. 6. (a) Optical spectra, (b) electrical spectra, and (c) phase noise characteristics of generated 120-GHz CW by photomixing output of photonic oscillator with suppression levels of optical carrier.

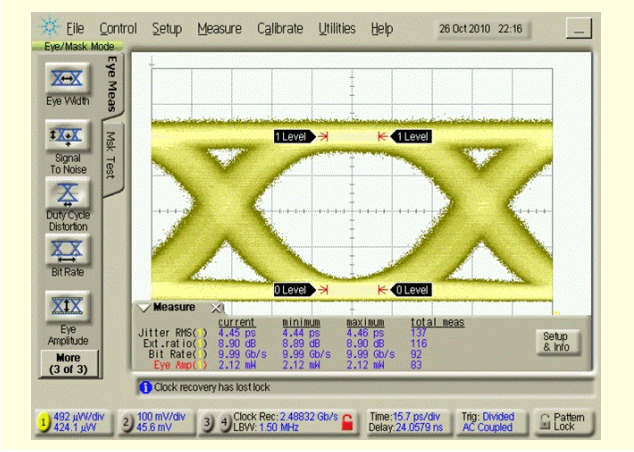

Fig. 7. Optical eye diagram of sub-THz Tx.

where R_{DC}, ρ, P_S, and Z_0 are the DC responsivity of the photomixer, the RF frequency response of the photomixer, the power of the DSBs, and the magnitude of the termination impedance of the ESA, respectively. The value of $P_{Ph,meas}$ agrees well with those of $P_{Ph,Cal}$ and Read-Out. Accordingly, we find that our measurement setup is suitable for verifying the photonic oscillator.

Figure 6 shows the optical and electrical characteristics of the generated 120-GHz CW with the suppression levels of the optical carrier. In this figure, λ_C, λ_S, mag(λ_C)>mag(λ_S), and mag(λ_C)<mag (λ_S) are the wavelengths of the optical carrier and the DSB signals, a case in which the magnitude of the optical carrier is higher than that of the optical sidebands, and a case in which the optical carrier is sufficiently suppressed, respectively. The optical spectra of the output of the photonic oscillator with the suppression levels of the optical carrier are illustrated in Fig. 6(a). The wavelength difference between the DSBs is 0.96 nm (120 GHz) owing to the use of an LO with f_{LO}=60 GHz. The suppression levels of the optical carrier result from controlling the bias voltage of the IM. When the bias voltage is at the peak point of the transfer curve of the IM (mag(λ_C)>mag(λ_S)), there are no suppression levels of the optical carrier. When the bias voltage is at the null point of the transfer curve of the IM (mag(λ_C)<mag(λ_S)), the suppression levels of the optical carrier are maximized [29].

The photomixed output power and phase noise characteristics of the generated 120-GHz CW with the suppression levels of the optical carrier are illustrated in Figs. 6(a) and 6(c), respectively. The photomixed output power in the case of mag(λ_C)<mag(λ_S) is 24 dB higher than that in the case of mag(λ_C)>mag(λ_S). The phase noise in the case of mag(λ_C)<mag(λ_S) is also improved by about 22 dB at a frequency offset of 1 MHz in comparison with the case of mag(λ_C)>mag(λ_S). According to the calculation and measurement results shown in Figs. 5 and 6, it is important that

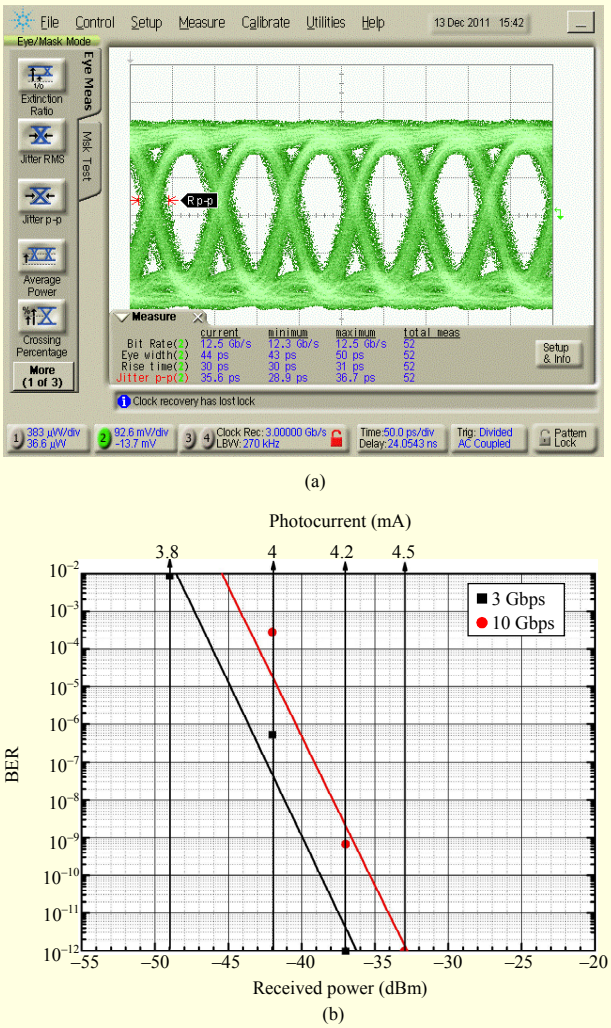

Fig. 8. (a) Eye diagram and (b) BER performances of sub-THz Rx for back-to-back connection between sub-THz Tx and sub-THz Rx.

the optical carrier should be sufficiently suppressed to improve the electrical and optical characteristics of the sub-THz CW generated by photomixing the output of the photonic oscillator.

The eye diagram measured at the output of the modulator is shown in Fig. 7. The modulator is composed of a DA, which is operated at 12 GHz of the 3-dB bandwidth and has a gain of 17 dB and a saturated output power of 22 dBm, and an IM that uses an MZI, which has a half-wave voltage of 3.5 V. The DSB-SC signals produced by the photonic oscillator are modulated with 10-Gbps NRZ PRBS 2^{31}–1 data. A desirable eye opening with a 4.44-ps jitter root mean square (RMS) and a 9-dB extinction ratio is observed.

Figure 8 shows back-to-back test results to verify the sub-THz Tx and sub-THz Rx. The sub-THz Rx is composed of the following: an SBD, which is a zero-bias detector, with an input of WR-08 waveguide, a coaxial output connector of 2.9 mm, a

responsivity of 2,800 V/W, an internal video resistance of 950 Ω, and a total capacitance of 40 fF at 120 GHz; an LNA with 5-V bias voltage, WR-08 waveguide input/output, a 1-dB compression point of –2 dBm, an upper 3-dB frequency of 122 GHz, and a 16-dB gain and 6-dB noise figure in the frequency range of 115 GHz to 125 GHz; a pre-amplifier with a 32-dB gain of up to 15 GHz; and a limiting amplifier operating at up to 12.5 Gbps as a post-amplifier.

The upper 3-dB cutoff frequency of the SBD and the pre-amplifier circuit is determined by (3) [31]:

$$f_{\mathrm{U(-3dB)}}\left(\mathrm{Hz}\right)=\frac{1}{2\pi\left(R_{\mathrm{V}}\parallel R_{\mathrm{L}}\right)C_{\mathrm{T}}}, \quad (3)$$

where C_{T} , R_{V}, and R_{L} are the total capacitance, the video resistance, and a load resistance. As the SBD is very fast and should operate over several tens of GHz, a shunt resistor of 50 Ω, the load resistance, is installed between the SBD and the pre-amplifier for impedance matching. To our knowledge, it is enough that the sub-THz Rx operates up to 10 Gbps.

To use the 120-GHz CW as a carrier frequency in the sub-THz range, the photomixer characterized in Fig. 5 is used. An isolator with a 3-dB insertion loss within the F-band is also installed between the photomixer and the Tx-antenna to prevent damage to the photomixer from the reflection waves. To measure the eye diagram and BER, 3-Gbps and 10-Gbps NRZ PRBS 2^{31}–1 data and 10-Gbps NRZ PRBS 2^{31}–1 data is applied to the modulator of the sub-THz Tx.

A desirable opening appears in the eye diagram of the sub-THz Rx with the 10-Gbps data, as shown in Fig. 8(a). As illustrated in Fig. 8(b), the received power, which is produced through photomixing the ASK-modulated DSB-SC signals, is measured at the end of the isolator by the ESA and HM. The photocurrent with the output power of the photonic oscillator is read out from the photomixer of the sub-THz Tx. It accordingly corresponds to the ASK-modulated output power of the sub-THz Tx. Using 3-Gbps NRZ PRBS 2^{31}–1 data and 10-Gbps NRZ PRBS 2^{31}–1 data, 3 Gbps and 10 Gbps are the back-to-back test results, respectively. The receiver sensitivity in the case of 3 Gbps and 10 Gbps is –37 dBm and –34 dBm at BER=10^{-12}, respectively. A penalty of 3 dB can be caused by the impedance mismatch between the SBD and the pre-amplifier and the gain flatness characteristics of the LNA. The gain flatness characteristics of an LNA should generally be below 1 dB within the required bandwidth for data transmission to guarantee dynamic performances [32]. In the case of 3-Gbps and 10-Gbps transmission, the required bandwidth is about 1.5 GHz and 5 GHz, respectively, when the NRZ data format is used. With a 120-GHz center frequency, the gain flatness of the LNA is over 3 dB in the 5-GHz bandwidth (117.5 GHz to 122.5 GHz) while being about 1 dB in the 1.5-GHz bandwidth. According to the back-to-back test results, it is confirmed that the designed sub-THz Tx and Rx operate normally.

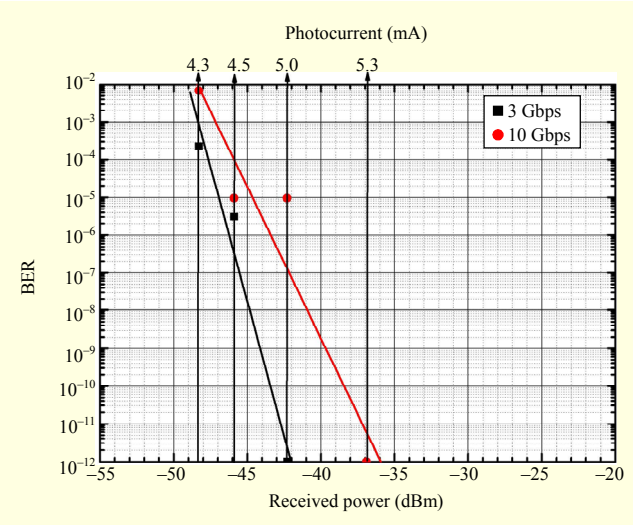

Fig. 9. BER results of high-speed wireless link with 3-m distance between sub-THz Tx and sub-THz Rx.

Table 1. Specifications of demonstrated high-speed wireless link based on photonics.

Sub-THz Tx	
Sub-THz CW	
Center frequency	120 GHz
–3-dB bandwidth	0.2 MHz
Modulation scheme	ASK
Modulation data	0.8 $V_{p\text{-}p}$ NRZ PRBS 2^{31}–1
Data rate	10 Gbps
Output power (max.)	–10 dBm
Tx-antenna	
Type	Cassegrain
Gain	46.5 dBi
Sidelobe	18 dB
–3-dB bandwidth	0.57°
Sub-THz Rx	
Bandwidth	10 GHz
Output voltage	0.4 $V_{p\text{-}p}$ (single-ended)
Sensitivity	–37 dBm (@ 10 Gbps BER=10^{-12})
Rx-antenna	
Type	Cassegrain
Gain	46.5 dBi
Sidelobe	18 dB
–3-dB bandwidth	0.57°

Without any error corrections, we perform a high-speed

wireless link test with a link distance of 3 m between the sub-THz Tx and sub-THz Rx. The BER test results for this link distance of 3 m are shown in Fig. 9. Table 1 also shows the specifications of the demonstrated high-speed wireless link. In Fig. 9, 3 Gbps and 10 Gbps are the back-to-back test results using 3-Gbps NRZ PRBS 2^{31}–1 data and 10-Gbps NRZ PRBS 2^{31}–1 data, respectively. The receiver sensitivity for 3 Gbps and 10 Gbps is respectively –41 dBm and –37 dBm at BER=10^{-12}. We suppose that the slope difference shown in Fig. 9 comes from a measurement error due to an alignment mismatch between the sub-THz Tx and sub-THz Rx with a link distance of 3 m.

Compared to the back-to-back test results shown in Fig. 8(b), the photocurrents of the photomixer for 3 Gbps and 10 Gbps increase from 4.2 mA to 5.0 mA and from 4.5 mA to 5.3 mA, respectively. Accordingly, the penalty caused by the loss of air at the link distance of 3 m between the sub-THz Tx and sub-THz Rx is about 0.8 mA. This means that the photomixer of the sub-THz Tx needs about 0.8 mA higher power to achieve BER=10^{-12} in comparison with the back-to-back test results.

The wireless link distance and receiver sensitivity can be improved when some error correction and a precise alignment algorithm between the sub-THz Tx and sub-THz Rx are applied. In accordance with the performance results, we find that the high-speed wireless link using the sub-THz wave generated by the photonics-based technology has the potential for a fixed wireless access of at least10 Gbps.

IV. Conclusion

In this paper, a high-speed wireless link using a sub-terahertz (THz) wave generated using photonics-based technology was designed and demonstrated to achieve the feasibility of sub-THz technologies for communication applications. The designed and demonstrated high-speed wireless link is composed of a sub-THz transmitter (Tx) and sub-THz receiver (Rx). The sub-THz Tx consists of a photonic oscillator, a modulator, and a sub-THz generator. The sub-THz Rx is an envelope detector consisting of a Schottky barrier diode and amplifiers. The photonic oscillator of the sub-THz Tx is configured based on the usual double sideband-suppressed carrier scheme. From the optical and electrical characterization results of the generated sub-THz wave, we have clearly defined that an optical carrier should be suppressed to obtain high photomixed output power with low phase noise characteristics. To verify a high-speed wireless link, such dynamic performances as an eye diagram and BER were measured for a back-to-back test and a link test with a link distance of 3 m between the sub-THz Tx and sub-THz Rx. From our measurement results, the receiver sensitivity for a link test with a link distance of 3 m is –37 dBm (@ BER=10^{-12}) with 10 Gbps non-return-to-zero pseudorandom binary sequence 2^{31}–1 data. For a link test with a link distance of 3 m, the sub-THz Tx has a 0.8 mA power penalty in comparison with the back-to-back test. The wireless link distance between the sub-THz Tx and sub-THz Rx can be extended with some error corrections and a precise alignment algorithm between the sub-THz Tx and sub-THz Rx. Consequently, we found that a high-speed wireless link using a sub-THz wave generated through photonics-based technology has the potential to realize a fixed wireless data link of over 10 Gbps, such as a seamless connectivity between wireless and wired networks, and high quantity transfer systems for indoor applications, such as high-definition multimedia and entertainment media.

References

[1] M.J. Fitch and R. Osiander, "Terahertz Waves for Communications and Sensing," *Johns Hopkins APL Technical Digest*, vol. 25, no. 4, 2004, pp. 348-355.

[2] M. Tonouchi, "Cutting-Edge Terahertz Technology," *Nature Photon.*, vol. 1, no. 2, Feb. 2007, pp. 97-105.

[3] TeraView, Ltd., terahertz products. www.teraview.com/products/index.html

[4] Y. Ogawa et al., "Terahertz Sensing for Ensuring the Safety and Security," *PIERS Online*, vol. 4, no. 3, 2008, pp. 396-400.

[5] M. Koch, *Terahertz Communications: A 2020 Vision*, New York: Springer, 2007.

[6] T. Kosugi et al., "mm-Wave Long-Range Wireless Systems," *IEEE Microw. Mag.*, vol. 10, issue 2, Apr. 2009, pp. 68-76.

[7] H.-J. Song et al., "Broadband-Frequency-Tunable Sub-terahertz Wave Generation Using an Optical Comb, AWGs, Optical Switches, and a Uni-traveling Carrier Photodiode for Spectroscopic Applications," *J. Lightw. Technol.*, vol. 26, no. 15, Aug. 2008, pp. 2521-2530.

[8] M.J. Fice et al., "Telecommunications Technology-Based Terahertz Sources," *Electron. Lett. — Special Supplement: Terahertz Technol.*, Dec. 2010, pp. S28-S31.

[9] T. Bryllert et. al., "11% Efficiency 100GHz InP-Based Heterostructure Barrier Varactor Quintupler," *Electron. Lett.*, vol. 41, no. 3, Feb. 2005, pp. 131-132.

[10] A. Maestrini, "Frequency Multipliers for Local Oscillators at THz Frequencies," *4th ESA Workshop Millimetre Wave Technol. Appl.*, Feb. 2006, pp.1-6.

[11] T.W. Crowe, D.W. Porterfield, and J.L. Hesler, "Multiplier-Based Sources of Terahertz Power," *33rd Int. Conf. Infrared, Millimeter, Terahertz Waves (IRMMW-THz)*, 2008.

[12] H. Eisele, "State of the Art and Future of Electronic Sources at Terahertz Frequencies," *Electron. Lett.-Special Supplement: Terahertz Technol.*, Dec. 2010, pp. S8-S11.

[13] B. Razavi, "A 300-GHz Fundamental Oscillator in 65-nm CMOS Technology," *IEEE J. Solid-State Circuits*, vol. 46, no. 4, Apr. 2011, pp. 894-903.

[14] W. Deal et al., "THz Monolithic Integrated Circuits Using InP High Electron Mobility Transistors," *IEEE Trans. Terahertz Sci. Technol.*, vol. 1, no. 1, Sept. 2011, pp. 25-32.

[15] Q.J. Gu et al., "CMOS THz Generator with Frequency Selective Negative Resistance Tank," *IEEE Trans. Terahertz Sci. Technol.*, vol. 2, no. 2, Mar. 2012, pp. 193-202.

[16] A. Maestrini et al., "Design and Characterization of a Room Temperature All-Solid-State Electronic Source Tunable from 2.48 to 2.72 THz," *IEEE Trans. Terahertz Sci. Technol.*, vol. 2, no.2, Mar. 2012, pp. 177-185.

[17] D. Saeedkia and S. Safavi-Naeini, "Terahertz Photonics: Optoelectronic Techniques for Generation and Detection of Terahertz Waves," *J. Lightw. Technol.*, vol. 26, no. 15, Aug. 2008, pp. 2409-2423.

[18] G. Scalari et al., "Electrically Switchable, Two-Color Quantum Cascade Laser Emitting at 1.39 and 2.3 THz," *Appl. Physics Lett.*, vol. 88, no. 14, Apr. 2006, pp. 141102-1-141102-3.

[19] C. Worrall et al., "Continuous Wave Operation of a Superlattice Quantum Cascade Laser Emitting at 2 THz," *Optical Express*, vol. 14, no. 1, Jan. 2006, pp. 171-181.

[20] G. Scalari et al., "THz and Sub-THz Quantum Cascade Lasers," *Laser & Photon. Rev.*, vol. 3, no. 1-2, 2009, pp. 46-66.

[21] J. Faist and G. Scalari, "Unified Description of Resonant Tunneling Diodes and Terahertz Quantum Cascade Lasers," *Electron. Lett.-Special Supplement: Terahertz Technol.*, Dec. 2010, pp. S46-S49.

[22] L.N. Langley et al., "Packaged Semiconductor Laser Optical Phase-Locked Loop (OPLL) for Photonic Generation, Processing and Transmission of Microwave Signals," *IEEE Trans. Microw. Theory Tech.*, vol. 47, no. 7, July 1999, pp. 1257-1264.

[23] J.E. Bjamason et al., "ErAs:GaAs Photomixer with Two-Decade Tenability and 12 uW Peak Output Power," *Appl. Physics Lett.*, vol. 85, no. 18, Nov. 2004, pp. 3983-3985.

[24] A. Hirata et al., "120-GHz-Band Millimeter-Wave Photonics Wireless Link for 10-Gb/s Data Transmission," *IEEE Trans. Microw. Theory Tech.*, vol. 54, no. 5, May 2006, pp. 1937-1944.

[25] T. Nagatsuma, "Terahertz Communications Technologies Based on Photonics and Electronics Approaches," *European Wireless*, Apr. 2012, pp. 1-4.

[26] J.J. O'Reilly et al., "Optical Generation of Very Narrow Linewidth Millimeter Wave Signals," *Electron. Lett.*, vol. 28, no. 25, Dec. 1992, pp. 2309-2311.

[27] X. Yu, H. Zhang, and X. Zheng, "High Carrier Suppression Double Sideband Modulation Using Polarization State Rotation Filter and Optical External Modulator," *Opt. Commun.*, vol. 267, no. 1, 2006, pp. 84-87.

[28] M. Tani et al., "Generation of Terahertz Radiation by Photomixing with Dual- and Multiple-Mode Lasers," *Semicond. Sci. Technol.*, vo. 20, no. 7, July 2005, pp. S151-S163.

[29] S. Kim and K.-Y. Kang, "Controlling Polarization of an Optical Carrier of Double Sideband-Suppressed Carrier Modulated Lightwave for Improving Characteristics of a Sub-terahertz Continuous Wave Generated by Photomixing," *Microw. Optical Technol. Lett.*, vol. 53, no. 3, Mar. 2011, pp. 626-630.

[30] R.T. Hawkins II et al., "Comparison of Fast Photodetector Response Measurements by Optical Heterodyne and Pulse Response Techniques," *J. Lightw. Technol.*, vol. 9, no. 10, Oct. 1991, pp. 1289-1294.

[31] Hewlett-Packard Application Note 923, *Schottky Barrier Diode Video Detectors*, Hewlet Packard, Nov. 1999.

[32] S.-F. Chao et al., "A DC-11.5-GHz Low-Power, Wideband Amplifier Using Splitting-Load Inductive Peaking Technique," *IEEE Microw. Wireless Compon. Lett.*, vol. 18, no. 7, July 2008, pp. 482-484.

Sungil Kim received his BS, MS, and PhD in electronics engineering from Ajou University, Suwon, Rep. of Korea, in 1995, 1997, and 2008, respectively. In 1997, he was with Hyundai Electronics Co., Ltd. (currently the SK Hynix Inc.), Rep. of Korea, as a research engineer in the field of high-speed interconnections design. From 1997 to 2000, he was with LG Electronics Co., Ltd., Seoul, Rep. of Korea, as a staff research engineer in the fields of high-speed interconnections design and electromagnetic interference. Since 2000, he has been with ETRI, Daejeon, Rep. of Korea, as a principal researcher. His current interests lie in the fields of design, testing, and characterization of terahertz devices and systems, SoC, SoP, high-speed optoelectronics, and EMI/EMC/high-speed interconnections for digital applications. *ETRI Journal* awarded him the Best Paper Award in 2008. He is a member of IEEE, IEEK, and KEES.

Seong-Ho Ahn received his BS and MS from Chonnam National University, Kwangju, Rep. of Korea, in 1986 and 1988, respectively, and his PhD in information and communications engineering from the Korea Advanced Institute of Science and Technology (KAIST), Daejeon, Rep. of Korea, in 2010. Since September 1989, he has been with ETRI, Daejeon, Rep. of Korea. His current research interests include optical connectors, optical interconnections, and optical backplane systems.

Seong Su Park received his BS in metallurgy from Yonsei University, Seoul, Rep. of Korea, in 1984, and his MS and PhD in materials science from the Korea Advanced Institute of Science and Technology (KAIST), Daejeon, Rep. of Korea, in 1986 and 1992, respectively. In 1993, he joined ETRI, Daejeon, Rep. of Korea. Until 2006, his areas of research were CMOS RFICs, MMICs, and high-speed optical device packaging. Since 2007, his area of research has been searching for and planning of future technologies.